VERSITA

Acta Geophysica
DOI: 10.2478/s11600-009-0028-3

Estimation of Orographically Induced Wave Drag in the Stable Boundary Layer during the CASES-99 Experimental Campaign

Gert-Jan STEENEVELD[1], Carmen J. NAPPO[2], and Albert A.M. HOLTSLAG[1]

[1]Department of Meteorology and Air Quality,Wageningen University, Wageningen, The Netherlands
e-mails: gert-jan.steeneveld@wur.nl (corresponding author), Bert.Holtslag@wur.nl

[2]CJN Research Meteorology, Knoxville, TN, USA; e-mail: cjn_met@comcast.net

Abstract

This paper addresses the quantification of gravity wave drag due to small hills in the stable boundary layer. A single column atmospheric model is used to forecast wind and temperature profiles in the boundary layer. Next, these profiles are used to calculate vertical profiles of gravity wave drag. Climatology of wave drag magnitude and "wave drag events" is presented for the CASES-99 experimental campaign. It is found that gravity wave drag events occur for several relatively calm nights, and that the wave drag is then of equivalent magnitude as the turbulent drag. We also illustrate that wave drag events modify the wind speed sufficiently to substantially change the surface sensible heat flux.

Key words: stable boundary layer, wave drag, orography, CASES-99.

1. INTRODUCTION AND BACKGROUND

The atmospheric boundary layer is that atmospheric layer that undergoes a diurnal cycle as a result of the diurnal cycle at the land surface, and that responds on a time scale of an hour or less (Stull 1988). At night, the nocturnal or stable boundary layer (SBL) develops as a result of longwave radiative cooling, which provides a surface temperature drop and a build up of

stable stratification. While turbulence is the main contributor to the daytime transport, the turbulence decays after the evening transition, and limits the nighttime turbulent transport. As a result, other physical processes than turbulence will become relevant in the SBL. These processes are, amongst others, drainage flows (e.g., Sun *et al.* 2004), radiation divergence (e.g., Hoch *et al.* 2007, Drüe and Heinemann 2007, Steeneveld *et al*. 2008c), intermittent turbulence (e.g., Mahrt 1989), the interaction with the land surface (e.g., Steeneveld *et al*. 2008b), and gravity waves (e.g., Nappo 1991, Brown and Wood 2003, Nappo and Svensson 2008). The simultaneous action of all these processes hampers our ability to understand and model the SBL, and the interpretation of measurements in the SBL is limited.

Atmospheric models for weather, climate and air quality encounter substantial problems in forecasting the nocturnal boundary layer (Cuxart *et al.* 2006, Beare *et al.* 2006, Bechtold *et al.* 2008, Bravo *et al.* 2008, Bosveld *et al.* 2008). Typical errors are the overestimation of the surface and screen level minimum temperature, the underestimation and the dislocation of the so-called nocturnal wind maximum (Steeneveld *et al.* 2008a, Storm *et al.* 2009), and the overestimation of magnitude of the turbulence intensity. This is a strong disadvantage for air quality forecasts (Salmond and McKendry 2005), climate studies based on reanalysis projects, and for end users in agriculture, (road and air) traffic and wind energy engineering (Storm *et al.* 2009). Hence, further research to the atmospheric physical processes is essential to improve future model performance.

A more specific deficiency of NWP model forecasts is the apparent need for enhanced turbulent surface drag compared to observed turbulent drag from field campaigns (e.g., Beare *et al.* 2006). Without additional drag, first, the skill scores for the large scale flow, i.e. the representation of the 500 hPa geopotential height, decrease in the medium and long range forecast. Second, some models experienced unphysical runaway cooling at the surface. Unfortunately, the physical processes that could possibly explain the additionally required drag are unknown. Steeneveld *et al.* (2008a) illustrated that the orographically induced gravity wave drag, which is supported in stably stratified conditions, may under idealized conditions partly explain the requested additional friction in models. Hence, this will allow for a reduction of the turbulent drag in these models, which will support further reduction of the model deficiencies. Also, a model study of McCabe and Brown (2007) showed that the apparent additional drag is correlated with the presence of orography.

Beyond the role of gravity wave drag in the SBL, another unexplained phenomenon in the SBL is worth investigation. In the intermediate atmospheric regime where the mechanical forcing (pressure gradient) and radiative cooling are of relatively equal importance, the so-called global intermittent

turbulence, and oscillations of wind speed and temperature have been reported (e.g., Nappo 1991, van de Wiel 2002, Acevedo and Fitzjarrald 2003, Steeneveld and Holtslag 2009). As an example, Fig. 1 shows the observed surface sensible heat flux for the night of 23/24 Oct. during the CASES-99 experimental campaign (Poulos *et al.* 2002). Periods with a large flux alternate with periods without any flux. This effect has not been incorporated in NWP models, and this misrepresentation may contribute to the poor model performance for the SBL (e.g., Dethloff *et al.* 2001).

Businger (1973) suggests as a possible explanation that increased stratification limits turbulent mixing, resulting in a reduced surface drag, which then causes flow acceleration by the pressure gradient force. Then a recoupling of the flow to the surface, and thus a re-initiation of turbulent friction may develop. Alternatively, Nappo (1991) found that propagating gravity waves can alter the local Richardson number below its critical value, temporarily allowing for turbulence.

As an alternative explanation for intermittent behaviour of the turbulence, we examine the role of orographically induced gravity wave drag on the SBL (e.g., Chimonas and Nappo 1989) and on intermittency in particular. In the linear theory, gravity wave propagation occurs when the Scorer parameter $L^2 = N^2 / U^2 - U'' / U^2 > k_s^2$, with stratification N, and k_s the wave number of the terrain topography.

We hypothesize that a sudden onset of (not turbulent) orographic wave drag occurs when $L^2 > k_s^2$, which then alters the total surface friction. Next, the turbulent friction is modified via the wind speed. As such, this may serve as an alternative explanation of the observed intermittency of turbulence intensity. In addition, the SBL is known for its inertial oscillation of the wind speed and direction (van Ulden and Wieringa 1996, Baas *et al.* 2009). As a

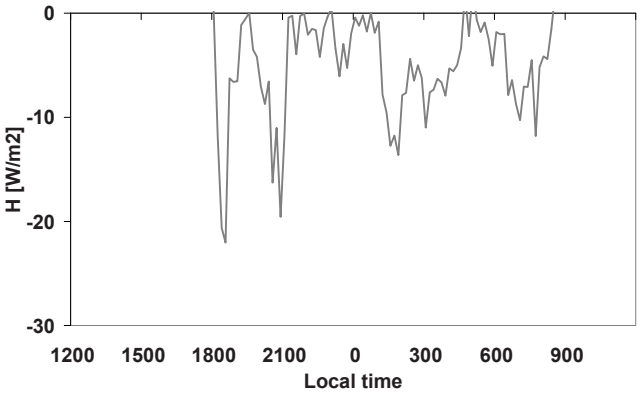

Fig. 1. Observed surface sensible heat flux for 23/24 Oct. 1999, during CASES-99.

result, one expects that within a certain night the flow will meet different obstacles, mountains or hills, with different amplitude and wavelength. Therefore, it should not be surprising that the wave drag can be variable in time within a single night. The aim of this paper is twofold. First, we quantify the gravity wave drag for CASES-99 in an innovative way and compare with observed turbulent drag. Secondly, we will investigate the role of orographically induced gravity wave drag on the triggering of intermittent turbulence. The remainder of the paper is organized as follows. Section 2 provides a theoretical background on gravity wave drag and an explanation of our innovative approach. Section 3 summarizes the available observations and terrain properties, and in Section 4 the experimental set-up is presented. Section 5 presents our results, and the paper will be closed by some conclusions and recommendations.

2. THEORY

Stratified flows allow for gravity wave propagation (Einaudi and Finnigan 1981). This can be horizontally propagating waves, triggered by any disturbance (e.g., hills, surface roughness transitions). However, in the current paper we limit ourselves to orographically induced waves. In stationary conditions, mountains or ridges can generate stationary gravity waves in a stably stratified medium. The role of propagating gravity waves in the SBL dynamics is under discussion (e.g., Finnigan 1999, Brown *et al.* 2003). Although specific knowledge of waves in the SBL is limited, there is sufficient observational (e.g., Kurzeja *et al.* 1991, Nappo 1991, Sun *et al.* 2004, Cheng and Brutsaert 2005) and theoretical (Chimonas and Nappo 1989, Nappo and Chimonas 1992, Belcher and Wood 1996) evidence to suggest that gravity waves are relevant. Since gravity waves generate wave stress, they might play an important role on the dynamical evolution of the SBL (Einaudi and Finnigan 1981, Finnigan 1999). This mechanism has been well understood for large mountain ridges. However, the SBL is shallow, and one can expect that also small-scale orography can significantly influence the SBL flow through gravity wave propagation. Nappo (2002) and Chimonas and Nappo (1989) indeed theoretically showed that the magnitude of the SBL wave stress and turbulent stress are of the same order during weak winds.

To further illustrate the relevant processes, Fig. 2 depicts the interactions of the mean variables, wind speed and stratification in the SBL on one hand, and the exchange processes on the other hand. In case wave drag is present (i.e., the condition $N/U > k_s$ has been fulfilled, see below), an increase in wind speed will increase the wave drag and provide additional friction to the PBL. Then a reduced wind speed will reduce the wave drag, but also the

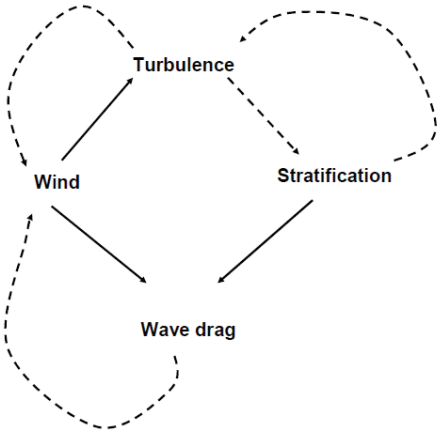

Fig. 2. Flow chart of interactions between the state variables (wind speed and stratification) and the exchange processes (wave drag and turbulence intensity). Full lines: positive feedback; dashed lines: negative feedback.

turbulence intensity, and thus increase the stratification. As a consequence, increased stratification will increase the wave drag, but will reduce the turbulent exchange. As such, the net result on the wind speed is a subtle balance between processes.

As a first estimate, the wave drag for an idealized sinusoidal surface corrugation for constant wind speed and stratification is given by (Belcher and Wood 1996, Nappo 2002)

$$\tau_{\text{wave}} = \frac{1}{2}\rho_0 k_s (U H_{\text{oro}})^2 \sqrt{N^2/U^2 - k_s^2}\ , \tag{1}$$

if $N/U > k_s$. Here N is the Brunt–Väisälä frequency $(N = \sqrt{g\nabla_z\theta/\theta})$, H_{oro} the orography amplitude, k_s the wave number, ρ_0 the air density, and U the background wind speed perpendicular to the orography.

So far, we did not account for the complexity of real terrain, i.e., irregular hills. For this more complex terrain, eq. (1) is not valid, but eq. (1) is valid for each wave component of the Fourier transform of the terrain when U and N are constant. Then, an alternative approach to estimate τ_{wave} for these conditions is to use a high-resolution 3D (mesoscale) model that is able to resolve τ_{wave} for the dominant wave numbers (Mauritsen *et al.* 2005, Steeneveld *et al.* 2008a). The disadvantage of this approach is that contributions by small wave numbers are neglected due to the still relatively coarse model resolution compared to the terrain. To ensure mesoscale model parameterizations still produce reliable results, one should avoid resolutions smaller than ~1 km, while in reality orographic perturbations on a smaller

horizontal scale have shown to contribute to τ_{wave}. Using a mesoscale model, one also relies on land use and topographic information that is delivered with the model. This information is not always available and optimized for high resolutions that are required to resolve the wave perturbations in the SBL. Finally, mesoscale model simulations are computationally expensive which limits the possibility to develop climatology or long term estimates of τ_{wave}. For these reasons, we apply a different approach here.

In this paper, we use the linear wave theory to estimate the area averaged surface wave drag (Shutts 1995, Nappo and Svensson 2008). The difficulty that arises for realistic terrain is that only the wind speed component perpendicular to each hill will generate a gravity wave. Each horizontal projection of the surface wind will pass over terrain features that will launch gravity waves, and each horizontal projection defines a wave vector. The total wave field is the sum of the waves by each of these projections. Thus, the wave perturbations should be calculated (i.e., the Taylor–Goldstein equation should be solved, assuming constant wind direction with height) for all wind components ϕ within $\pm\pi/2$ of the surface wind direction.

In case the wind direction changes with height, which is highly likely in the SBL, it might occur that at a certain level, the background wind vanishes for a certain wave vector. Then wave dissipation at this critical level reduces the wave perturbation to practically zero.

As for idealized terrain, and assuming formation of standing waves, the approach starts solving the Taylor–Goldstein equation for each wind sector ϕ (with $\hat{w}$ the Fourier transform of the vertical wind speed; Nappo and Svensson 2008):

$$\frac{\mathrm{d}^2}{\mathrm{d}z^2}\hat{w}_\phi(k_s,z)+\left[\frac{N^2}{U_\phi^2}-\frac{U_\phi''}{U_\phi}-k_s^2\right]\hat{w}_\phi(k_s,z)=0\,. \tag{2}$$

As a surface boundary condition we use $\hat{w}_\phi(0)=-\mathrm{i}\,k\hat{u}_\phi(0)\,\hat{h}_\phi(k_s)$. The perturbation of the horizontal wind speed follows from the continuity equation and reads as $\hat{u}_\phi=\dfrac{\mathrm{i}}{k_s}\dfrac{\partial\hat{w}_\phi}{\partial z}$. To account for the non idealized terrain, these perturbations are calculated for 36 wind sectors of 10º. Finally, the contributions to τ_{wave} from all sectors are added to provide the area averaged wave drag. For further details on the applied method, we refer to Chapter 9 of Nappo (2002) and Nappo and Svensson (2008).

It should be mentioned here that the validity of the linear theory under current conditions is not a priori valid. However, Steeneveld *et al.* (2008a) showed that the linear theory provides reasonable estimates for surface wave drag in high-resolution MM5 simulations over moderate topography.

3. METEOROLOGICAL OBSERVATIONS AND TERRAIN CHARACTERISTICS

For this study we select the period 6-27 October 1999 during the CASES-99 campaign (Poulos *et al.* 2002), which has partly been analyzed before in the context of a column and mesoscale model study in Steeneveld *et al*. (2006, 2008a). The experiment has been conducted near Leon, Kansas, USA (37.65ºN, 96.73ºW, 436 m asl). The area consists of a prairie-grass vegetation on a gently rolling homogeneous terrain with a relatively dry soil, and lacks obstacles in the near surroundings. Although this region is often referred to as relatively flat, Fig. 3 shows that several undulations are present in this area. The standard deviation of the terrain height amounts ~7 m, as obtained from the USGS (http://seamless.usgs.gov/website/seamless/viewer.htm) data.

Ground based observations consist of θ, q and wind profiles along a 60 m tower (mounted at 1.5, 5, 10, …, 55 m), and turbulent and radiative fluxes near the surface. The eddy-covariance measurements of the surface sensible heat flux H, latent heat flux $L_v E$, and friction velocity u_* were obtained at 2.6 m, using the eddy covariance software developed by van Dijk *et al*. (2004). The surface energy budget closure is approximately 100% for these nights (Steeneveld *et al.* 2006). Additionally, irregularly launched radiosondes and tethered balloon flights provided information on upper air characteristics. Mini-sodar observations complete the wind speed observations below 200 m.

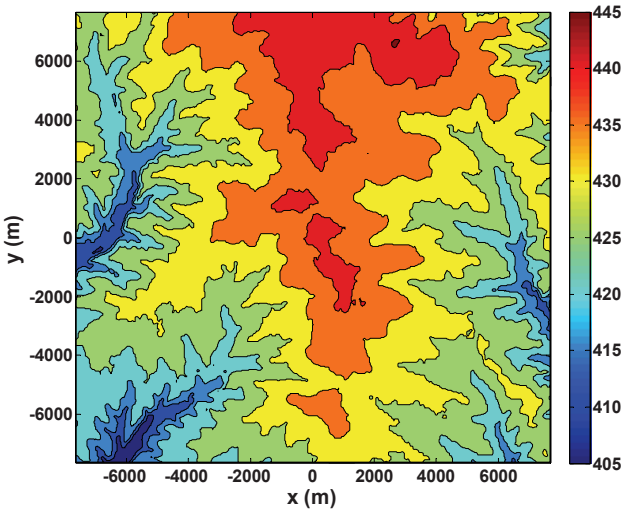

Fig. 3. Terrain height (m) around the CASES-99 terrain (central site is in the middle). Source: http://seamless.usgs.gov/website/seamless/viewer.htm), United States Geological Survey. Colour version of this figure is available in electronic edition only.

4. EXPERIMENTAL SET-UP

We perform a model study on wave drag for CASES-99, aiming on the identification of wave stress "events" and quantification of wave drag and comparison with turbulent drag ($\tau_{\text{turb}} = \rho u_*^2$). The single column model of Duynkerke (1991) is used to forecast the ABL wind speed and temperature profiles. This model has been validated against Cabauw tower observations and contrasting days in CASES-99 (Steeneveld *et al.* 2006), and showed good performance for the SBL, except for wind and temperature oscillations and intermittent turbulence.

The column model utilizes a 1st order turbulence scheme for the turbulent diffusivity K,

$$K_x = \frac{(kz)^2}{\varphi_m \varphi_x} \left| \frac{\partial U}{\partial z} \right| \tag{3}$$

with flux profile relations (with $\alpha = 0.8,\ \beta_m = 5,\ \beta_h = 7.5$)

$$\varphi_x(\zeta) = \frac{kz}{X_*} \frac{\partial X}{\partial z} = 1 + \beta_x \zeta \left(1 + \frac{\beta_x}{\alpha_x} \zeta \right)^{\alpha_x - 1} \tag{4}$$

with $x = m$ for momentum, and $x = h$ for heat, and $\zeta = z/L$, with L the local Obukhov length. Also, a grey-body emissivity radiation scheme (Garratt and Brost 1981) and a full coupling with the soil (T_{soil}) and the vegetation (T_{veg}) is applied (Duynkerke 1991), for which the budget equation reads (Q^* is the net radiation and $C_{\text{veg}} = 2000\ \text{J m}^{-2}\text{K}^{-1}$ is the heat capacity of the vegetation layer):

$$C_{\text{veg}} \frac{\partial T_{\text{veg}}}{\partial t} = Q^* - H - L_v E - \Lambda \left(T_{\text{veg}} - T_{\text{soil}} \right), \tag{5}$$

in which the soil heat flux is represented by the last term, which utilizes soil conductance Λ. For the current model runs we use $\Lambda = 5.0\ \text{Wm}^{-2}\text{K}^{-1}$, although the numerical value of Λ is relatively uncertain, since $2.5 < \Lambda < 7.0\ \text{W m}^{-2}\text{K}^{-1}$ in several studies (e.g., van Ulden and Holtslag 1985, Viterbo and Beljaars 1995, Duynkerke 1999, Cupido 2002, van de Wiel 2002, Steeneveld *et al.* 2006). This large uncertainty of Λ is of key importance, because Λ plays a vital role in the evolution of the SBL stratification (e.g., Steeneveld *et al.* 2006), which may affect the calculated wave drag.

The model has a domain of 1800 m with a logarithmically spaced grid of about 0.5 m near the surface, and the model runs with a time step of 10 s. For the current model simulations, surface roughness length for momentum z_{0m} was taken to be 0.03 m, as observed for CASES-99, and the roughness length for heat $z_{0h} = z_{0m}/10$. The initial profiles for temperature and humidity

are taken from the 19:00 UTC (12:00 LT) radio sounding each day. The geostrophic wind speed ($\boldsymbol{U}_g$) was determined from the same sounding as a vertical average of the 5 observations closest to the 800 m agl. In this way, we circumvent possible biases in geostrophic wind due to outliers. $\boldsymbol{U}_g$ was kept constant in time and height, and nights with a non-stationary $\boldsymbol{U}_g$ have been excluded from the analysis below. Close to the surface, the initial wind speed was matched with a neutral logarithmic profile.

We would like to remark here that large-scale topographic effects caused by the slope of the Great Plains are not incorporated in our column model simulation, and therefore the low-level jet (LLJ) is not a priori adequately represented (Steeneveld *et al.* 2006). Despite this deficiency in the modelled LLJ, the near surface winds and stratification that control the surface wave drag can still be estimated in a reliable manner.

Next, the forecasted U and θ profiles are forwarded from the 1D column model to the wave drag scheme, as explained in Section 2 (Nappo and Svensson 2008). The wave drag scheme uses a vertical resolution of 10 m. For now, the wave stress divergence does not feed back to the wind tendency, and we only analyze the calculated surface wave drag in offline mode. However, below we will theoretically explain the role of wave drag on the near surface wind, and sensible heat flux. It should be realized that in case the wave drag divergence feeds back on the mean flow, as might occur in reality, the offline approach is not valid anymore. This will be discussed further below.

In addition to the reference runs, we explore the sensitivity of the calculated wave stress to the model settings, we vary the heat conductance Λ , the coefficients in eq. (5), and $\boldsymbol{U}_g$ as a sensitivity test.

Note that we use model-based wind and temperature profiles to force the wave drag calculation in this experiment. In principle, we also could have adopted an alternative strategy to use observational data from the 60 m tower, wind profiler, kite, sodar, and radio soundings to construct $U(z,t)$ and $\theta(z,t)$ fields for the full CASES-99 experiment. However, radio soundings and kite observations were unfortunately not regularly available at a high temporal resolution, while the other instruments were limited to low altitude (e.g., < 200 m). Also, the near surface radio sounding wind observations showed relatively high degree of missing data. In addition, near surface observations may cover features that are not of particular interest for this study, e.g., phenomena that occur on a smaller horizontal scale than the wavelength of the orography (e.g., drainage flows). Including these small scale disturbances could provide spurious results on the scale of interest, which should be avoided. Therefore, it was impossible to construct reliable $U(z,t)$ and $\theta(z,t)$ fields for all nights. For this reason, we adopted our current approach.

5. RESULTS

5.1 Model validation

Since the meteorological profiles that are used for the wave drag computations are essential for the resulting τ_{wave}, we first briefly provide some further validation of the modelled wind speed and temperature profiles on the selected case studies that will be shown below.

We have decided to focus our analysis on the selected nights of 9/10, 19/20, 20/21, and 25/26 October 1999, and we will compare the model forecast with observations of the 07:00 UTC (01:00 local time) sounding (see Fig. 4). For the last night we evaluate against the 03:00 UTC (22:00 LT) sounding, because the 07:00 UTC sounding was missing. For the night of

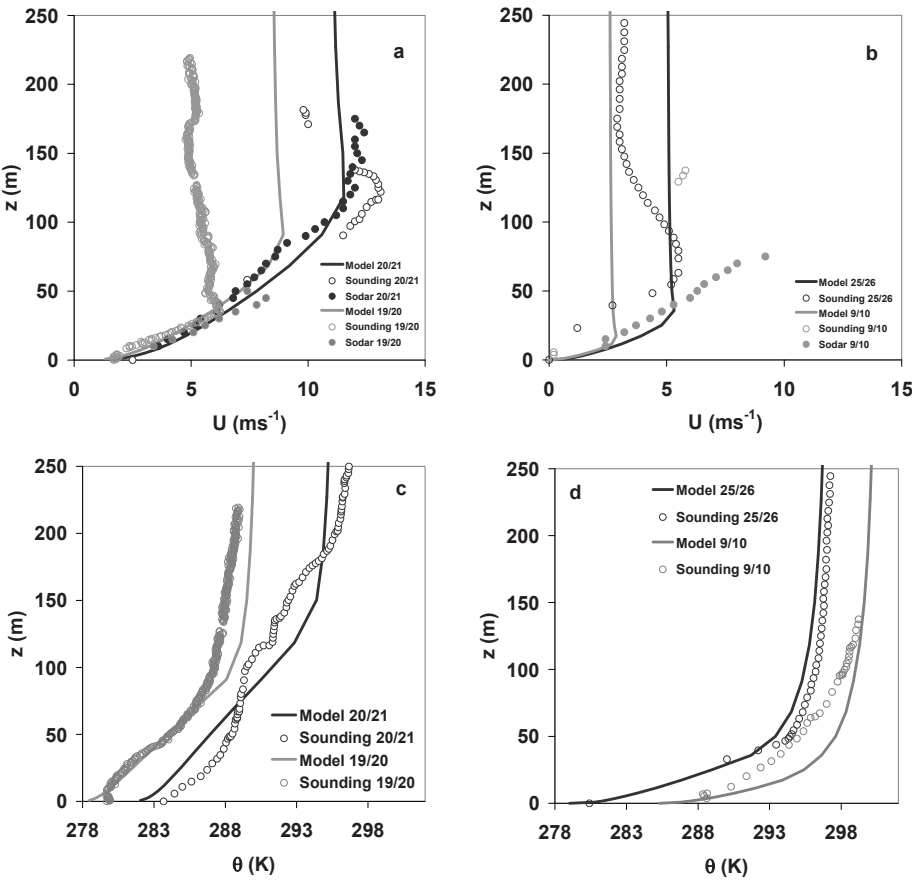

Fig. 4. Modelled and observed (radio soundings and sodar) wind speed (panels a and b) and potential temperature profiles (panels c and d) at 7:00 UTC (1:00 LT) (3:00 UTC or 22:00 LT for 25/26 October) for the CASES-99 central site.

19/20 October the modelled temperature profile corresponds well with the tethered balloon observations, although the model is approximately 1 K warmer above the SBL than observed. The wind speed profile is successfully modelled below the LLJ, which itself is modelled at a slightly too low altitude. However, the LLJ wind speed is strongly underestimated by approximately 4 m s^{-1}, which agrees with findings in Steeneveld *et al.* (2006). For 20/21 October similar performance is found as for the previous night, although the LLJ and temperature above the SBL are slightly better reproduced. In the radiative night of 25/26 October the modelled temperature matches with the observations. Unfortunately, the SBL wind shear has been overestimated by the model, the LLJ height is underestimated, and the baroclinicity above the SBL is not well forecasted, since the modelled wind is 2 m s^{-1} higher than observed. Finally for 9/10 October, the temperature is overestimated between 5 and 150 m by at maximum 2 K, although the surface temperature and residual layer temperature is correct. In this case the estimated wind speed is underestimated, as is the LLJ. Of course, one should be aware that the results depend in principle on the applied forcing. Therefore, Section 5.2.1 will study the sensitivity of the results to the chosen $\boldsymbol{U}_g$.

Conclusively, the performance of the column model on wind speed and stratification is of sufficient quality to use its results for the wave stress calculations, especially taking account the current state of the art of SBL modelling.

5.2 Wave drag

5.2.1 Individual nights

Next we will discuss the time series of calculated surface wave drag for the selected nights. A full overview of calculated wave drag for all nights is presented in Table 1. For each night, the $\boldsymbol{U}_g$ and the classification by van de Wiel (2002) for that particular night has been mentioned (i.e., Turbulent, Intermittent, Radiative or Non). Note this classification was based on visual inspection of the measured surface sensible heat fluxes.

For the intermittent clear night of 19/20 October, with an $\boldsymbol{U}_g$ of 7.6 m s^{-1}, intermittent behaviour of wave stress is modelled, with a typical time scale of 1-2 h (Fig. 5a). The typical value for τ_{wave} in the so-called "wave drag events" amounts ~–0.002 N m^{-2}, although a peak value of –0.0033 N m^{-2} is found. Between these events, long periods without wave activity occur (e.g., between $t = 33.5$ and 35 h). Also, the calculated magnitude of the wave stress events corresponds to the order of magnitude of the turbulent drag. In addition, the correspondence between the signal of the modelled τ_{wave} and observed τ_{turb} is striking. Since the wind and temperature fields from the column model do not show any intermittency, the wave drag events are generated completely ***independently*** by the wave module, and are the result of the

Table 1

Overview of modelled wave drag events, wave drag magnitude and character of the observed turbulent fluxes per night of October 1999. U_g and V_g are the geostrophic wind speed in x and y directions, respectively, U_{LLJ} is the wind speed magnitude of low-level jet, h_{LLJ} is the height of low-level jet.

Day	Wave drag events	Max wave drag [N m^{-2}] τ_x τ_y	U_g , V_g [m s^{-1}]	Van de Wiel (2002) class	U_{LLJ} [m s^{-1}]	h_{LLJ} 07:00 UTC
6/7	No	0, 0	0.6, 12.3	Turb	21.2	188
8/9	Yes	0, 0.006	–4.6, –0.8	–	9.5	65
9/10	Yes	–0.0033, 0.0035	2.1, –0.8	Rad	7.7	245
10/11	Yes	–0.0055, –0.0055	3.8, –0.6	Turb	17.6	136
11/12	Yes	0.0040, –0.002	3.1, 6.7	–	14.3	180
12/13	No	0, 0	7.1, 10.4	Non	20.4	193
14/15	No	0, 0	6.0, 8.7	Turb	28.4	124
15/16	No	0, 0	5.7, 19.4	–	15.5	246
16/17	No	0, 0	–8.6, –14.2	Turb		
17/18	No	–0.0016, 0	–0.7, –9.4	Int		
18/19	Yes	–0.0060, –0.002	4.7, –1.0	Rad	10.9	316
19/20	Yes	–0.0033, –0.0013	3.5, –6.4	Int		
20/21	Yes	0.0030, 0.0032	7.7, 5.2	Non	13.1	122
22/23	No	0, 0	4.5, –12.5	Non	18.5	176
23/24	Yes	–0.0060, 0	0.1, –6.1	Int	11.3	90
24/25	Yes	0.0035, –0.0018	–0.3, 0.9	Turb	17.4	134
25/26	Yes	–0.0040, 0	3.1, –2.3	Rad	–	–
26/27	Yes	0.0008, –0.0005	3.0, 5.0	Int	15.3	129

interaction between the SBL flow and the orography solely. As such, this result suggests confirmation of our hypothesis that wave drag may occur in events. Note that at this time we do not formulate an exact definition for a wave drag event, although this could possibly be done either relative to the mean wave drag during the night or relative to the total wind tendency. In a later stage of research on this subject, the formulation of a more rigorous formal definition is required to enable practical use in large-scale models.

For the night of 20/21 October we find that the wave drag is mostly active just in the transition (around 24:00 UTC ≈ 18:00 LT) (Fig. 5b), with peaks of 0.003 N m^{-2} and –0.003 N m^{-2} in the x and y directions, respectively. During this transition wave stress occurs in bursts that are separated ~1 h in time from each other. At that time, the observed turbulent momentum flux is of equal order of magnitude, but later on in that night the mean wind and turbulent momentum flux increase. Then the wave stress also vanishes.

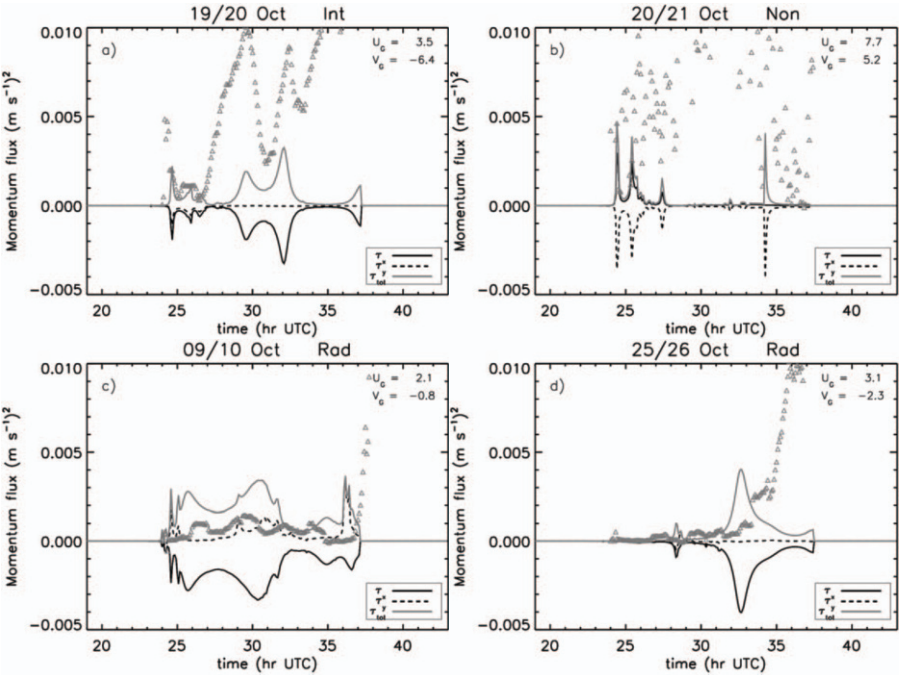

Fig. 5. Modelled surface wave stress components and total drag (lines), and measured total turbulent stress (triangles) for a series of nights in CASES-99. In the header the classification of van de Wiel (2002) (Turb, Rad, Non) is also indicated, (U_g, V_g) indicate the geostrophic wind for the simulation.

Although not shown here, we found that even for nights with negligible mean wave stress, some evident and substantial peaks in wave stress occur after the transition. This occurs for the nights of 11/12, 18/19, 23/24, and 26/27 October.

Despite the fact that the wave stress is not intermittent for the night of 9/10 October, this night is interesting in the series we discuss here because the wave stress is of more continuous nature. This night has a geostrophic wind speed of only ~2.5 m s^{-1}, and the observed turbulent fluxes are extremely small. However, Fig. 5c shows that the modelled surface wave drag is substantial, and that its magnitude is as large as the turbulent flux. Thus, for this type of nights, the gravity wave drag seems to be an integral part of the SBL physics. Therefore, it is likely that the current offline approach for the wave drag calculation is not valid anymore for this night. The relatively large wave drag and its vertical divergence can in reality impact on the wind speed via the momentum budget equation, and one should use an online approach to account for this.

Finally, Fig. 5d shows the model results for the radiative night from 25/26 October in which the observed turbulent fluxes vanish in the first part of the night. Then also the wave stress is small, with some wave drag events of ~0.0005 N m^{-2}. However, at midnight (t ~30 h), the near surface wind speed increases, and generates both turbulent stress and wave stress of comparable magnitude. τ_{wave} is limited to one event of substantial drag in the x direction of $\tau_{wave} = -0.006$ N m^{-2}. In addition to the intermittent behaviour of the wave stress, we also find in general that the magnitude of the wave stress is larger for the x direction than for the y direction. This is due to the fact that in general the terrain wavelength is larger in the x direction than in the y direction.

Table 1 shows that wave drag is nonzero at least 50% of the nights, preferably in the relatively calm nights, although in some turbulent nights the τ_{wave} is also substantial. Unfortunately, we do not find any obvious relation between τ_{wave} and geostrophic wind speed, LLJ height or speed, except that τ_{wave} vanishes for $\boldsymbol{U}_g > 10$ m s^{-1}. As such, simple parameterization seems not possible.

5.5.2 Sensitivity to surface interaction

The calculated wave drag depends both on wind speed and near surface stratification via the Scorer parameter on one hand, and via eq. (1) directly on the other hand. We hypothesize that the calculated wave stress depends on the near surface wind and stratification. Both are controlled by the coupling between the soil temperature and vegetation temperature. Therefore, a sensitivity test is performed on the value of Λ. We ran the model for $\Lambda = 5.9$ Wm^{-2}K^{-1} (as previously reported), and for $\Lambda = 4.5$ Wm^{-2}K^{-1} as an alternative.

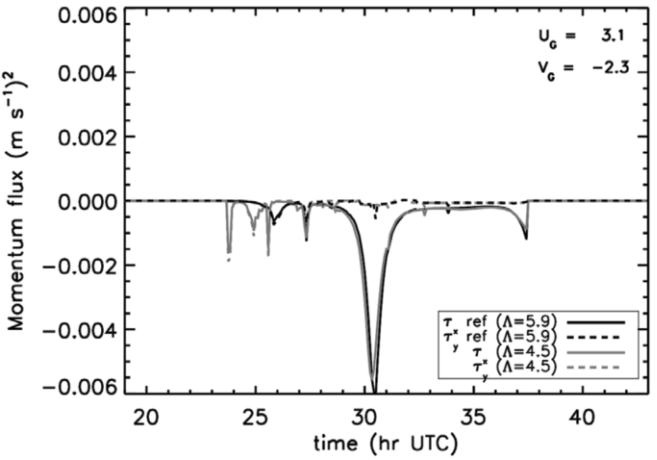

Fig. 6. Modelled surface wave stress components for 25/26 October in CASES-99. Reference $\Lambda = 5.9$ Wm^{-2}K^{-1}, alternative $\Lambda = 4.5$ Wm^{-2}K^{-1}.

Figure 6 shows the results for the night of 9/10 October. Intercomparing the two runs, we find that low Λ results in a similar amount of wave stress, except that in the early night more events occur, although their numerical value is small. This means that, at least for this night, the U profile is a more limiting factor for τ_{wave} than is the stratification.

5.2.3 Sensitivity to profile functions

Since the wave propagation is regulated by the Scorer parameter that is determined itself by θ and U profiles, one also may expect certain sensitivity to the chosen form of the flux-profile relations in the ABL model. The functional form of the flux-profile relations is under debate. Substantially different forms have been proposed by different authors, based on different field experiments (e.g., Beljaars and Holtslag 1991, Andreas 2002, Cheng and Brutsaert 2005). These uncertainties occur, amongst other, due to instrumental problems in stable conditions (e.g., application of the eddy covariance technique in stable conditions is difficult because wind speed and temperature perturbations are small and difficult to detect accurately), and mesoscale flows. In addition, spurious correlation is known to affect ϕ_m and ϕ_h for the SBL (Klipp and Mahrt 2004, Baas *et al.* 2006). Figure 7 shows for 25/26 October the results using $\beta_h = \beta_m = 4$ in eq. (1). Our general finding is (also for other nights, not shown) that the functional form of the flux-profile relations provides a time shift of the wave stress events, but only slightly alters the wave stress magnitude. This robustness of the results provides further confidence in the relevance of the proposed mechanism.

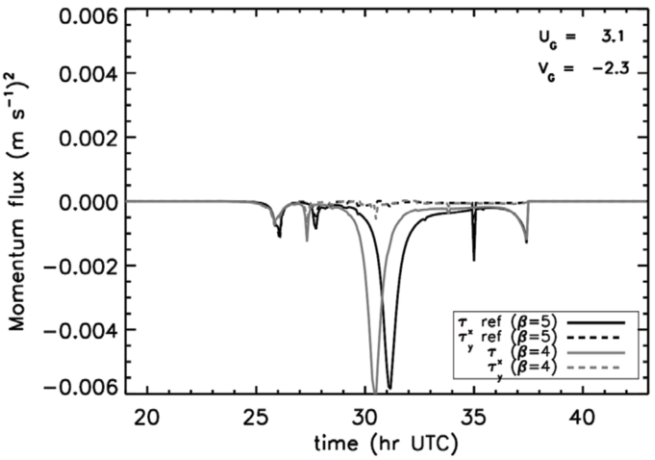

Fig. 7. Modelled surface wave stress components for different profile functions (see text) for 25/26 October in CASES-99.

5.2.4 Sensitivity to geostrophic wind speed

The geostrophic wind speed determines dominantly the flow in our simulations in the column model, and is as such a governing variable for the wind speed and stratification near the surface (Estournel and Guedalia 1985). Unfortunately, $\boldsymbol{U}_g$ is difficult to determine accurately from field observations, or from radio soundings only. As an alternative, Bosveld *et al.* (2008) were successful in estimating $\boldsymbol{U}_g$ speed using the observed pressure field, though such a network is not available for the current situation. In this paragraph we illustrate the sensitivity of our results to the choice of the $\boldsymbol{U}_g$ on the calculated orographic drag. For the simulation of the night of 9/10 October, Fig. 8 shows the results for τ_{wave} using a halved and doubled $\boldsymbol{U}_g$ as was found from the 800 m wind speed (keeping the direction of $\boldsymbol{U}_g$ similar). For the halved geostrophic wind, the τ_{wave} remains continuously nonzero during the night, but is reduced from –0.002 N m^{-2} to typically –0.0005 N m^{-2} in the x direction. For the doubled $\boldsymbol{U}_g$, the $\tau_{\text{wave.x}}$ is not continuous anymore, but concentrated in four events. Especially substantial events occur at $t = 32$ h and $t = 37$ h, each with a larger drag than for the reference geostrophic wind speed. Remarkable is the sign change of the wave drag in the y direction. To summarize, we find a strong sensitivity of the calculated τ_{wave} to the geostrophic wind speed.

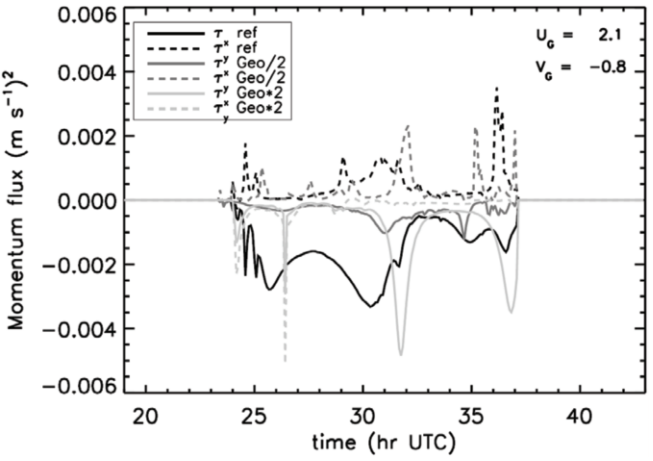

Fig. 8. Calculated gravity wave drag for the night of 9/10 October 1999, using simulations with the reference geostrophic wind, and with a halved and doubled geostrophic wind speed.

5.3 Impact of wave drag on turbulent fluxes

Next we analyze the consequence of a sudden onset of wave drag on the surface sensible heat flux. Let us consider a wave drag event of $\tau_{\text{wave}} = 0.003$ N m^{-2}

that lasts for 1 h in an environment of $U = 2$ m s^{-1}, with $u_* = 0.07$ m s^{-1} (inspired on the night of 25/26 October). We assume, as in Steeneveld *et al.* (2008a), that the wave dissipation occurs over a SBL depth h. One can estimate the SBL depth using the empirical formula $h = \alpha u_*$, with $\alpha = 700$ s (Vogelezang and Holtslag 1996), which results in $h = 49$ m. This means that the wind speed reduction in this hour amounts to

$$\Delta U = \int_0^{1hr} -\partial|\tau| \Big/ \partial z \, \mathrm{d}t \approx 0.25 \text{ m s}^{-1}.$$

Figure 9 shows the sensible heat flux as a function of the implied temperature difference ΔT between the surface and the reference level, using Monin–Obukhov similarity theory (Delage *et al.* 2002, Holtslag *et al.* 2007). For a small ΔT, a ΔT increase results in larger $|H|$, since in this regime the turbulent intensity is not yet limited by the stratification. However, for larger ΔT (at the right side of the minimum of H), the stratification is so strong that turbulence starts to be reduced, and as such H also declines for a ΔT increase. A reduction of the wind speed with 0.25 m s^{-1} results in a substantial reduction of the surface sensible heat flux magnitude, especially in a broad regime around $\Delta T = 5$ K. As such, this illustrates the potential impact on a tiny wave stress on the turbulent fluxes.

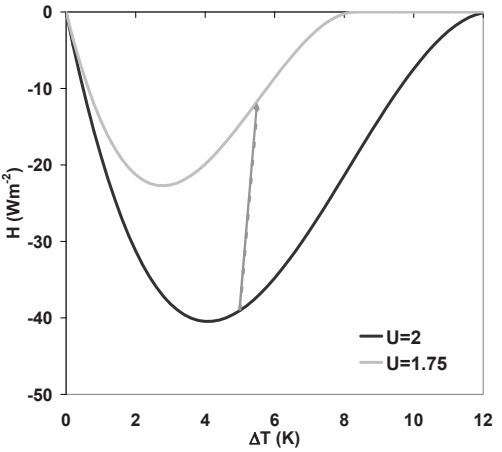

Fig. 9. Sensible heat flux H as a function of temperature difference between the surface and the reference level, for two different wind speeds.

In the previous analysis ΔT was taken constant when we stepped from $U = 2$ m s^{-1} to $U = 1.75$ m s^{-1}, but in reality one expects that ΔT will increase after a $|H|$ reduction. At the same time, it can be found from solving a simplified surface energy budget equation that

$$\frac{\mathrm{d}T_{\mathrm{veg}}}{\mathrm{d}U}=\frac{\rho C_p T_a C_H(\varepsilon_s\sigma T_{\mathrm{ref}}^3+\Lambda+\rho C_p T_a U)-(L^{\downarrow}+\Lambda T_s+\rho C_p T_a U)\rho C_p C_H}{(\varepsilon_s\sigma T_{\mathrm{ref}}^3+\Lambda+\rho C_p C_H U)^2}. \quad (6)$$

Herein, T_a, T_s, and T_r are the air, soil and reference temperatures, respectively, $L^{\downarrow}$ the prescribed longwave downwelling radiation (~300 Wm^{-2} for this case), ε_s the surface emissivity (taken as 1.0), C_H the exchange coefficient for heat (taken constant ~2×10^{-3} for the illustrative purpose of this analysis), ρ and C_p are the density and heat capacity of air at constant pressure. Equation (6) explains that while we reduce the wind speed, due to wave stress, the surface energy budget constraints require a decrease of the surface temperature, and thus an increase in ΔT. For the described atmospheric conditions, $\mathrm{d}T_{\mathrm{veg}}/\mathrm{d}U$ ~2.2 K/(m s^{-1}), which explains the slope of the grey dashed line in Fig. 9, which represents trajectory that will be followed. Note, however, that $\mathrm{d}T_{\mathrm{veg}}/\mathrm{d}U$ increases rapidly in case $U\rightarrow 0$, and thus a stronger sensitivity occurs for weak winds, which will result in a steeper slope of the dashed line in Fig. 9. As a secondary effect, the reduced wind will also reduce u_*, and thus will reduce the turbulent exchange even more, and as a positive feedback ΔT will increase.

6. DISCUSSION

Some aspects of the above results need further attention. First of all, the coupling of the column model and the wave stress module is non-trivial. One may question what is the appropriate surface wind speed to force the wave module. For the real surface wind (i.e., 0 m s^{-1}) no wave stress will occur. For wind speed higher in the boundary layer, wave stress does occur, but one should question whether this is really the wind speed that is felt by the orography. Belcher and Wood (1996) propose that the wind speed at the "middle layer height" gives the best results compared to detailed model simulations.

Secondly, the current simulations do not take into account the possible effect of wave saturation. This occurs when the wave perturbations grow to such amplitude that convective instabilities are possible. Then the wave perturbations are mixed away by the convection and as a consequence τ_{wave} is reduced. In that case, the wave dissipation will feedback to the wind field.

For a study with MM5 over the CASES-99 terrain, Steeneveld *et al.* (2008a) report a parabolic decrease of τ_{wave} with height, and especially over the SBL. The effect of wave saturation on τ_{wave} can be calculated using a terrain height adjustment scheme as in Chapter 9.2 of Nappo (2002). To circumvent convective overturning, the wave perturbations for the horizontal

wind $\tilde{u}$ are kept in a range such that $|\tilde{u}/U|<1$, by reducing the amplitude of the underlying orography iteratively by 5% each time. Tjernström *et al*. (2009) found a substantial reduction of the τ_{wave} in the SBL. As such, the inclusion of wave dissipation for the current calculations is a very interesting subject for further research.

It is worth noting that Böing (2009) found substantial degree of intermittent turbulence in DNS model simulations. To mimic the characteristics of vegetation friction, Böing (2009) prescribed the drag coefficient as tangent-hyperbolic with height in his simulations. At the level of sudden decrease of the drag coefficient, i.e., a critical level was implied and turbulence was generated. Although these results cannot a priori be translated one to one to the atmosphere, they provide an additional potential mechanism for the onset of intermittent turbulence. At the same time, it supports our hypothesis that a drag divergence close to the surface plays a role in intermittent oscillations.

We showed that accounting for wave drag can reduce the surface sensible heat flux for calm conditions, which supports surface cooling. However, the enhanced turbulent mixing in operational models is also applied to avoid run away surface cooling. Thus, inclusion of wave drag instead of the unphysical enhanced turbulent mixing seems to partly counteract the effect we want to achieve. However, a realistic description of each physical process in the SBL should be preferred. The surface cooling problem indicates that further attention should also be paid to understanding radiative transport and the role of the land surface in the SBL.

As a final remark, we would like to stress that we proposed an alternative mechanism for intermittency of turbulence. However, it does not automatically mean that other possible mechanisms, such as described in Businger (1973) and van de Wiel (2002), propagating non-orographic gravity waves, or intermittent mixing from the shear layer below the LLJ are disqualified. The future challenge is to quantify and classify the atmospheric conditions under which each of these processes contribute to intermittent mixing, and finally to parameterize them in atmospheric models for weather, climate and air quality.

7. CONCLUSIONS

In this paper, we analyze the possible role of orographically induced gravity wave drag in comparison with turbulent drag in the stable boundary layer. Since the stable boundary layer is relatively shallow, one may expect that already modest orography of hills and ridges can affect the stable boundary layer temporal and vertical structure. An innovative method is used to estimate the surface wave drag based on single column model forecasts of tem-

perature and wind speed. This is done for nearly all nights during the CASES-99 field campaign.

For relatively weak winds, the surface gravity wave drag occurs in "wave drag events" with a timescale that corresponds to that of the observed global intermittency and wind speed and temperature oscillations. This finding indicates that wave drag events could possibly also contribute to the frequently observed temperature and wind speed oscillations in the stable boundary layers. We show, using Monin–Obukhov similarity theory, that the time scale of the wave drag events can reduce the near surface wind speed sufficiently to initiate a substantial reduction of the surface sensible heat flux magnitude. Although this is not a final explanation of intermittency, it may contribute to further understanding of the phenomenon.

Finally, especially for the calm nights, the calculated surface wave drag appears to be of similar magnitude as the observed turbulent drag. This suggests that orographic drag is an integral part of the SBL physics for these calm nights, and need to be parameterized in NWP and climate models.

Acknowledgements. G.J. Steeneveld acknowledges the BSIK-ME2 project (Climate changes spatial planning), and we thank our colleague Dr. O.K. Hartogensis (Wageningen University) for gathering and providing the CASES-99 turbulent flux observations. The United States Geological Survey is acknowledged for the making available the U.S. topographical information at http://seamless.usgs.gov/website/seamless/viewer.htm.

References

Andreas, E.L. (2002), Parameterizing scalar transfer over snow and ice: A review, *J. Hydrometeorol.* **3**, 4, 417-432, DOI: 10.1175/1525-7541(2002)003<0417:PSTOSA>2.0.CO;2.

Acevedo, O.C., and D.R. Fitzjarrald (2003), In the core of the night-effects of intermittent mixing on a horizontally heterogeneous surface, *Bound.-Layer Meteor.* **106**, 1, 1-33, DOI: 10.1023/A:1020824109575.

Baas, P., G.J. Steeneveld, B.J.H. van de Wiel, and A.A.M. Holtslag (2006), Exploring self-correlation in flux-gradient relationships for stably stratified conditions, *J. Atmos. Sci.* **63**, 11, 3045-3054, DOI: 10.1175/JAS3778.1.

Baas, P., F.C. Bosveld, H. Klein Baltink, and A.A.M. Holtslag (2009), A climatology of nocturnal low-level jets at Cabauw, *J. Appl. Meteorol. Clim.*, DOI: 10.1175/2009JAMC1965.1.

Beare, R.J., M.K. MacVean, A.A.M. Holtslag, J. Cuxart, I. Esau, J.-C. Golaz, M.A. Jimenez, M. Khairoutdinov, B. Kosovic, D. Lewellen, T.S. Lund, J.K. Lundquist, A. McCabe, A.F. Moene, Y. Noh, S. Raasch, and P. Sullivan (2006), An intercomparison of Large-Eddy Simulations of the stable boundary layer, *Bound.-Layer Meteor.* **118**, 2, 247-272, DOI: 10.1007/s10546-004-2820-6.

Bechtold, P., M. Köhler, T. Jung, F. Doblas-Reyes, M. Leutbecher, M.J. Rodwell, F. Vitart, and G. Balsamo (2008), Advances in simulating atmospheric variability with the ECMWF model: From synoptic to decadal time-scales, *Quart. J. Roy. Met. Soc.* **134**, 634, 1337-1351, DOI: 10.1002/qj.289.

Belcher, S.E., and N. Wood (1996), Form and wave drag due to stably stratified turbulent flow over low ridges, *Quart. J. Roy. Met. Soc.* **122**, 532, 863-902, DOI: 10.1002/qj.49712253205.

Beljaars, A.C.M., and A.A.M. Holtslag (1991), Flux parameterization over land surfaces for atmospheric models, *J. Appl. Meteorol*. **30**, 3, 327-341, DOI: 10.1175/1520-0450(1991)030<0327:FPOLSF>2.0.CO;2.

Böing, S. (2009), Intermittent turbulence in stratified flow over a porous canopy, MSc Thesis, Utrecht University, Utrecht, 68 pp.

Bosveld, F.C., E.I.F. de Bruijn, and A.A.M. Holtslag (2008), Intercomparison of single-column models for GABLS3 – preliminary results. **In:** *Proc. 18th Symposium on Boundary Layer and Turbulence, 9-13 June 2008, Stockholm*, paper 8A.5.

Bravo, M., T. Mira, M.R. Soler, and J. Cuxart (2008), Intercomparison and evaluation of MM5 and Meso-NH mesoscale models in the stable boundary layer, *Bound.-Layer Meteor.* **128**, 1, 77-101, DOI: 10.1007/s10546-008-9269-y.

Brown, A.R., and N. Wood (2003), Properties and parameterization of the stable boundary layer over moderate topography, *J. Atmos. Sci*. **60**, 22, 2797-2808, DOI: 10.1175/1520-0469(2003)060<2797:PAPOTS>2.0.CO;2.

Brown, A.R., M. Athanassiadou, and N. Wood (2003), Topographically induced waves within the stable boundary layer, *Quart. J. Roy. Met. Soc.* **129**, 595, 3357-3370, DOI: 10.1256/qj.02.176.

Businger, J.A. (1973), Turbulent transfer in the atmospheric surface layer. **In:** D.A. Haugen (ed.), *Workshop on the Planetary Boundary Layer*, Amer. Meteor. Soc., 67-98.

Chenge, Y., and W. Brutsaert (2005), Flux-profile relationships for wind speed and temperature in the stable atmospheric boundary layer, *Bound.-Layer Meteor.* **114**, 3, 519-538, DOI: 10.1007/s10546-004-1425-4.

Chimonas, G., and C.J. Nappo (1989), Wave drag in the planetary boundary layer over complex terrain, *Bound.-Layer Meteor.* **47**, 1-4, 217-232, DOI: 10.1007/BF00122330.

Cupido, D. (2002), *Estimation of Surface Energy Fluxes from Single-Level Weather Data for the Wageningen Weather Station*, Wageningen University, Wageningen, The Netherlands, 52 pp.

Cuxart, J., A.A.M. Holtslag, R.J. Beare, E. Bazile, A.C.M. Beljaars, A. Cheng, L. Conangla, M. Ek, F. Freedman, R. Hamdi, A. Kerstein, H. Kitagawa, G. Lenderink, D. Lewellen, J. Mailhot, T. Mauritsen, V. Perov, G. Schayes, G.-J. Steeneveld, G. Svensson, P.A. Taylor, W. Weng, S. Wunsch, and K.M. Xu (2006), Single-column model intercomparison for a stably stratified atmospheric boundary layer, *Bound.-Layer Meteor.* **118**, 2, 273-303, DOI: 10.1007/s10546-005-3780-1.

Delage, Y., P.A. Barlett, and J.H. McCaughey (2002), Study of 'soft' night-time surface-layer decoupling over forest canopies in a land-surface model, *Bound.-Layer Meteor.* **103**, 2, 253-276, DOI: 10.1023/A:1017443021557.

Dethloff, K., C. Abegg, A. Rinke, I. Hebestadt, and V.F. Romanov (2001), Sensitivity of Arctic climate simulations to different boundary-layer parameterizations in a regional climate model, *Tellus* **53A**, 1-26.

Drüe, C., and G. Heinemann (2007), Characteristics of intermittent turbulence in the upper stable boundary layer over Greenland, *Bound.-Layer Meteor.* **124**, 3, 361-381, DOI: 10.1007/s10546-007-9175-8.

Duynkerke, P.G. (1991), Radiation fog: A comparison of model simulation with detailed observations, *Monthly Weath. Rev.* **119**, 2, 324-341, DOI: 10.1175/1520-0493(1991)119<0324:RFACOM>2.0.CO;2.

Duynkerke, P.G. (1999), Turbulence, radiation and fog in Dutch stable boundary layers, *Bound.-Layer Meteor.* **90**, 3, 447-477, DOI:10.1023/A:1026441904734.

Einaudi, F., and J.J. Finnigan (1981), The interaction between an internal gravity wave and the planetary boundary layer. Part I: The linear analysis, *Quart. J. Roy. Met. Soc.* **107**, 454, 793-806, DOI: 10.1256/smsqj.45403.

Estournel, C., and D. Guedalia (1985), Influence of geostrophic wind on atmospheric nocturnal cooling, *J. Atmos. Sci*. **42**, 23, 2695-2698, DOI: 10.1175/1520-0469(1985)042<2695:IOGWOA>2.0.CO;2.

Finnigan, J. (1999), A note on wave-turbulence interaction and the possibility of scaling the very stable boundary layer, *Bound.-Layer Meteor.* **90**, 3, 529-539, DOI: 10.1023/A:1001756912935.

Garratt, J.R., and R.A. Brost (1981), Radiative cooling effects within and above the nocturnal boundary layer, *J. Atmos. Sci*. **38**, 12, 2730-2746, DOI: 10.1175/1520-0469(1981)038<2730:RCEWAA>2.0.CO;2.

Hoch, S.W., P. Calanca, R. Philipona, and A. Ohmura (2007), Year-round observation of longwave radiative flux divergence in Greenland, *J. Appl. Meteorol. Clim.* **46**, 9, 1469-1479, DOI: 10.1175/JAM2542.1.

Holtslag, A.A.M., G.J. Steeneveld, and B.J.H. van de Wiel (2007), Role of land-surface temperature feedback on model performance for the stable boundary layer, *Bound.-Layer. Meteor*. **125**, 2, 361-376, DOI: 10.1007/s10546-007-9214-5.

Klipp, C.L., and L. Mahrt (2004), Flux-gradient relationship, self-correlation and intermittency in the stable boundary layer, *Quart. J. Roy. Met. Soc.* **130**, 601, 2087-2103, DOI: 10.1256/qj.03.161.

Kurzeja, R.J., S. Berman and A.H. Weber (1991), A climatological study of the nocturnal planetary boundary layer, *Bound.-Layer Meteor.* **54**, 1-2, 105-128, DOI: 10.1007/BF00119415.

Mahrt, L. (1989), Intermittent of atmospheric turbulence, *J. Atmos. Sci*. **46**, 1, 79-95, DOI: 10.1175/1520-0469(1989)046<0079:IOAT>2.0.CO;2.

Mahrt, L. (2009), Characteristics of submeso winds in the stable boundary layer, *Bound.-Layer Meteor.* **130**, 1, 1-14, DOI: 10.1007/s10546-008-9336-4.

Mauritsen, T., G. Svensson, and B. Grisogono (2005), Wave flow simulations over Arctic leads, *Bound.-Layer Meteor.* **117**, 2, 259-273, DOI: 10.1007/s10546-004-1427-2.

McCabe, A. and A.R. Brown (2007), The role of surface heterogeneity in modelling the stable boundary layer, *Bound.-Layer Meteor.* **122**, 3, 517-534, DOI: 10.1007/s10546-006-9119-8.

Nappo, C.J. (1991), Sporadic breakdowns of stability in the PBL over simple and complex terrain, *Bound.-Layer Meteor*. **54**, 1-2, 69-87, DOI: 10.1007/BF00119413.

Nappo, C.J. (2002), *An Introduction to Atmospheric Gravity Waves*, Academic Press, 276 pp.

Nappo, C.J., and G. Chimonas (1992), Wave exchange between the ground surface and a boundary-layer critical level, *J. Atmos. Sci*. **49**, 13, 1075-1091, DOI: 10.1175/1520-0469(1992)049<1075:WEBTGS>2.0.CO;2.

Nappo, C.J., and G. Svensson (2008), A parameterization with wave saturation adjustment of subgrid-scale average wave stress over three-dimensional topography. **In:** *Proc. 18th Symposium on Boundary Layer and Turbulence, 9-13 June 2008, Stockholm*, paper 6A.2.

Poulos, G.S., W. Blumen, D.C. Fritts, J.K. Lundquist, J. Sun, S.P. Burns, C. Nappo, R. Banta, R. Newsom, J. Cuxart, E. Terradellas, B. Balsley, and M. Jensen (2002), Cases-99: A comprehensive investigation of the stable nocturnal boundary layer, *Bull. Am. Meteor. Soc.* **83**, 4, 555-581, DOI: 10.1175/1520-0477(2002)083<0555:Caciot>2.3.Co;2.

Salmond, J.A., and I.G. McKendry (2005), A review of turbulence in the very stable nocturnal boundary layer and its implications for air quality, *Prog. Phys. Geog.* **29**, 2, 171-188, DOI: 10.1191/0309133305pp442ra.

Shutts, G. (1995), Gravity-wave drag parametrization over complex terrain: The effect of critical-level absorption in directional wind-shear, *Quart. J. Roy. Met. Soc*. **121**, 525, 1005-1021, DOI: 10.1002/qj.49712152504.

Steeneveld, G.J., and A.A.M. Holtslag (2009), Meteorological aspects of air quality. **In:** G.C. Romano and A.G. Conti (eds.), *Air Quality in the 21st Century* (in press).

Steeneveld, G.J., B.J.H. van de Wiel, and A.A.M. Holtslag (2006), Modeling the evolution of the atmospheric boundary layer coupled to the land surface for three contrasting nights in CASES-99, *J. Atmos. Sci.* **63**, 3, 920-935, DOI: 10.1175/JAS3654.1.

Steeneveld, G.J., A.A.M. Holtslag, C.J. Nappo, B.J.H. van de Wiel, and L. Mahrt (2008a), Exploring the possible role of small-scale terrain drag on stable boundary layers over land, *J. Appl. Meteorol. Clim.* **47**, 10, 2518-2530, DOI: 10.1175/2008JAMC1816.1.

Steeneveld, G.J., T. Mauritsen, E.I.F. de Bruijn, J. Vilà-Guerau de Arellano, G. Svensson, and A.A.M. Holtslag (2008b), Evaluation of limited-area models for the representation of the diurnal cycle and contrasting nights in CASES-99, *J. Appl. Meteor. Clim*. **47**, 3, 869-887, DOI: 10.1175/2007 JAMC1702.1.

Steeneveld, G.J., C.D. Groot Zwaaftink, M.J.J. Wokke, S. Pijlman, B.G. Heusinkveld, A.F.G. Jacobs, and A.A.M. Holtslag (2008c), Long term observations of long wave radiative flux divergence in the stable boundary layer over land. **In:** *Proc. 18th Symposium on Boundary Layer and Turbulence, 9-13 June 2008, Stockholm*, paper 17.B6.

Storm, B., J. Dudhia, S. Basu, A. Swift, and I. Giammanco (2009), Evaluation of the weather research and forecasting model on forecasting low-level jets: Implications for wind energy, *Wind Energy* **12**, 1, 81-90, DOI: 10.1002/ we.288.

Stull, R.B. (1988), *An Introduction to Boundary-Layer Meteorology*, Kluwer Academic Publishers, Dordrecht.

Sun, J., D.H. Lenschow, S.P. Burns, R.M. Banta, R.K. Newsom, R. Coulter, S. Frasier, T. Ince, C.J. Nappo, B.B. Balsey, M. Jensen, L. Mahrt, D. Miller, and B. Skelly (2004), Atmospheric disturbances that generate intermittent turbulence in nocturnal boundary layers, *Bound.-Layer Meteor.* **110**, 2, 255-279, DOI: 10.1023/A:1026097926169.

Tjernström, M., B.B. Balsley, G. Svensson, and C.J. Nappo (2009), The effects of critical layers on residual layer turbulence, *J. Atmos. Sci.* **66**, 2, 468-480, DOI: 10.1175/2008JAS2729.1.

Van de Wiel, B.J.H (2002), *Intermittent turbulence and oscillations in the stable boundary layer over land*, PhD Thesis, Wageningen University, Wageningen, 129 pp.

Van Dijk, A., A.F. Moene, and H.A.R. de Bruin (2004), *The Principles of Surface Flux Physics: Theory, Practice and Description of the ECPACK Library*, Wageningen University Int. Report 2004/1, Wageningen, 99 pp.

Van Ulden, A.P., and A.A.M. Holtslag (1985), Estimation of atmospheric boundary layer parameters for diffusion applications, *J. Appl. Meteorol.* **24**, 11, 1196-1207, DOI: 10.1175/1520-0450(1985)024<1196:EOABLP>2.0.CO;2.

Van Ulden, A.P., and J. Wieringa (1996), Atmospheric boundary layer research at Cabauw, *Bound.-Layer Meteor.* **78**, 1-2, 39-69, DOI: 10.1007/BF00122486.

Viterbo, P., and A.C.M. Beljaars (1995), An improved land surface parameterization scheme in the ECMWF model and its validation, *J. Climate* **8**, 11, 2716-2748, DOI: 10.1175/1520-0442(1995)008<2716:AILSPS>2.0.CO;2.

Vogelezang, D.H.P., and A.A.M. Holtslag (1996), Evaluation and model impacts of alternative boundary-layer height formulations, *Bound.-Layer Meteor.* **81**, 3-4, 245-269, DOI: 10.1007/BF02430331.

Received 19 December 2008
Accepted 15 July 2009